Chemical Science

EDGE ARTICLE

Check for updates

AIE-active luminogens as highly efficient free-radical ROS photogenerator for image-guided photodynamic therapy†

Zhenxing Liu,[a] Qi Wang, [ID] *[a] Wanshan Qiu,[b] Yanting Lyu,[a] Zhirong Zhu,[a] Xiaolei Zhao[a] and Wei-Hong Zhu [ID] *[a]

Image-guided photodynamic therapy (PDT) can realize highly precise and effective therapy *via* the integration of imaging and therapy, and has created high requirements for photosensitizers. However, the PDT modality usually utilizes conventional type II photosensitizers, resulting in unsatisfactory imaging and therapeutic outcomes due to aggregation-caused quenching (ACQ), "always on" fluorescence and strong oxygen dependence. Herein, we report the type I-based aggregation-induced emission (AIE) photosensitizer TCM-CPS with low oxygen dependence, near-infrared (NIR) emission and "off–on" fluorescence; in particular, it produces more reactive oxygen species (ROS) than commercially available Chlorin e6 and Rose Bengal. In the rational design of the AIE-based photosensitizer TCM-CPS, the strongly electron-donating carbazole unit and π-thiophene bridge distinctly extend the emission wavelength and decrease the autofluorescence interference in bio-imaging, and the hydrophilic pyridinium salt group guarantees good molecular dispersion and maintains the fluorescence-off state in the aqueous system to decrease the initial fluorescence background. Moreover, the strong donor−π− acceptor (D−π−A) character in TCM-CPS greatly separates the HOMO−LUMO distribution, enhancing the ROS generation, and TCM-CPS was constructed as a type I photosensitizer with the assistance of strong intramolecular charge transfer in the electron-rich anion−π^+ structure. Based on its favorable hydrophilicity and photosensitivity, TCM-CPS was found to be a highly efficient free-radical ROS photogenerator for both visualizing cells using light-up NIR fluorescence and efficiently killing cancer cells upon light irradiation. The positively charged TCM-CPS could quickly bind to bacteria *via* electrostatic interactions to provide a light-up signal and kill bacteria at a low concentration. In the PDT treatment of bacteria-infected mice, the mice exhibited accelerated wound healing with low wound infection. Thus, the AIE-based type I photosensitizer TCM-CPS has great potential to replace commercially available photosensitizers in the image-guided PDT modality for the treatment of cancer and bacterial infection.

Introduction

Photodynamic therapy (PDT) is an emerging non-invasive modality to treat bacterial infection and cancer with several advantages, such as light-controlled area of treatment, low side effects and negligible drug resistance.[1–8] Image-guided PDT

[a]Shanghai Key Laboratory of Functional Materials Chemistry, Key Laboratory for Advanced Materials and Institute of Fine Chemicals, Joint International Research Laboratory of Precision Chemistry and Molecular Engineering, Feringa Nobel Prize Scientist Joint Research Center, Frontiers Science Center for Materiobiology and Dynamic Chemistry, School of Chemistry and Molecular Engineering, East China University of Science and Technology, Shanghai 200237, China. E-mail: whzhu@ecust.edu.cn; wangqi@ecust.edu.cn

[b]Department of Cardiothoracic Surgery, Children's Hospital of Fudan University, Shanghai 201102, China

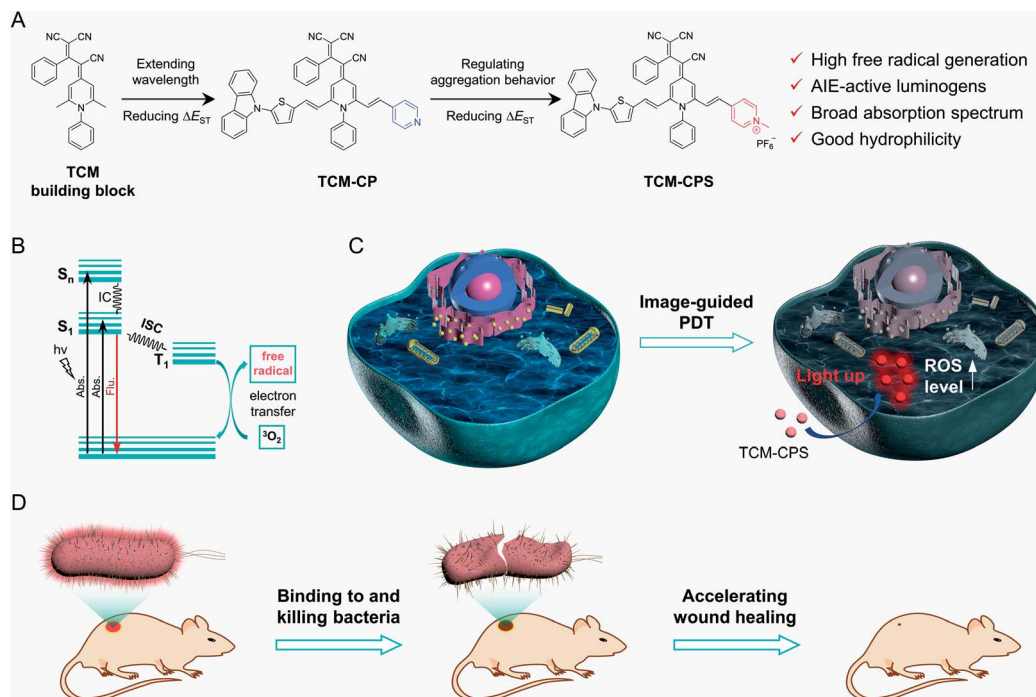† Electronic supplementary information (ESI) available. See DOI: 10.1039/d2sc00067a

could realize more precise and effective therapy *via* the integration of imaging and therapy, and introduces high requirements for photosensitizers.[9–11] However, conventional hydrophobic photosensitizers tend to aggregate in aqueous systems and show quenched fluorescence and decreased photosensitivity in the aggregated state.[12–14] Additionally, the "always on" fluorescence and small Stokes shift of these photosensitizers result in low signal-to-noise ratios (S/N) in bioimaging and visualization. In terms of therapy, these photosensitizers are always type II photosensitizers with strong oxygen dependence, which critically limit their application in hypoxia.[15,16] Therefore, there is an urgent need to develop a type I photosensitizer with both precise imaging capability and high reactive oxygen species (ROS) generation for image-guided PDT.

Aggregation-induced emission (AIE) photosensitizers have drawn great attention in image-guided PDT, since the restriction of intramolecular motion (RIM) can decrease the thermal

Fig. 1 Illustration of highly efficient free-radical ROS photogenerator for killing cancer cells and bacteria. (A) Rational design of the efficient photosensitizers. A carbazole, π-bridged thiophene, and pyridine group were used to extend the wavelength range and separate the HOMO–LUMO distribution to decrease the ΔE_{S1-T1} value of TCM. After forming the pyridinium salt, TCM-CPS was obtained with enhanced solubility, colloidal stability and photosensitivity in aqueous systems. (B) Mechanism of free-radical ROS generation after TCM-CPS is excited by light. (C) TCM-CPS could image cancer cells with light-up NIR fluorescence and generate ROS for killing cancer cells upon light irradiation. (D) TCM-CPS could bind to and kill bacteria upon light irradiation, as well as accelerate the wound healing process.

deactivation of their excited energy, resulting in bright fluorescence and enhanced photosensitivity in the aggregated state.[17–23] Recently, a feasible strategy based on strong intramolecular charge transfer (ICT) in electron-rich anion–π⁺ AIEgens was developed to design a type I photosensitizer, in order to reduce the oxygen dependence in PDT.[24] In addition, AIEgens with "off–on" fluorescence could realize higher-fidelity imaging compared to ACQ fluorophores, especially in terms of decreasing false fluorescence signals.[25–28]

Our group has reported the novel AIE building block TCM,[29,30] which has high fluorescence in the aggregated state, multiple modification sites, and good photostability; TCM is expected to be useful in the construction of photosensitizers through structural regulation (Fig. 1). Therefore, the hydrophilic type I photosensitizer TCM-CPS with near-infrared (NIR) emission and "off–on" fluorescence was developed for application in image-guided PDT. The strongly electron-donating carbazole unit and π-bridge of the thiophene group can realize strong intramolecular charge transfer (ICT) for redshifted emission in the NIR region, thus reducing the interference from background biological fluorescence for precise imaging.[31–34] The hydrophilic pyridinium salt group can maintain good miscibility of TCM-CPS in biological media, thus achieving desirable "off–on" fluorescence. Given that the pyridinium salt group and three cyano groups are very strong electron-withdrawing groups, the strong donor–π–acceptor (D–π–A) character of TCM-CPS can greatly separate the HOMO–

LUMO distribution to decrease ΔE_{ST}, thereby enhancing the intersystem crossing process (ISC) for higher ROS generation. Moreover, the electron-rich heteroatoms (S and N) provide electrons for producing free-radical ROS; thus, the obtained electron-rich anion–π⁺ AIEgens with strong ICT would be efficient free-radical ROS photogenerators.

TCM-CPS exhibits a broad absorption spectrum, which is very beneficial for matching the white light spectrum. Moreover, the ROS generation of TCM-CPS is much higher than that of the commercial photosensitizers Rose Bengal (RB) and Chlorin e6 (Ce6), predominantly producing free-radical ROS. Based on its high hydrophilicity and photosensitivity, TCM-CPS could penetrate and image cells with light-up NIR fluorescence and produce free-radical ROS to effectively kill tumor cells upon light irradiation, making it very useful for image-guided PDT at the cellular level. Furthermore, the positively charged photosensitizer TCM-CPS could bind to negatively charged bacteria through electrostatic interactions with "off–on" fluorescence and simultaneously produce a strong bactericidal effect upon light irradiation, which accelerated the wound healing process of mice.

Results and discussion

Developing an AIE-active luminogen for use as a highly efficient free-radical ROS photogenerator

AIE photosensitizers have drawn great attention in image-guided PDT because of their bright fluorescence and

enhanced photosensitivity in the aggregated state, which could allow them to realize excellent imaging and therapeutic effects.[35–37] TCM, which was reported by our group, is a typical AIE building block with a classic D–π–A structure, and is expected to be useful in the construction of photosensitizers through rational structural design. The incorporation of the strongly electron-donating carbazole unit and π-bridged thiophene group in TCM-CP was aimed at simultaneously realizing a strong ICT system for red-shifted emission and separated HOMO–LUMO distribution for ROS generation. A strongly electron-withdrawing and hydrophilic pyridinium salt group was then introduced to further separate the HOMO–LUMO distribution for higher ROS generation, as well as to guarantee

good molecular dispersion in an aqueous system, thereby regulating the aggregation behavior for the fluorescence-off state. In this way, the strong D–π–A structure in TCM-CPS can not only ensure strong ICT for NIR emission, but also greatly separate the HOMO–LUMO distribution for high ROS production. The synthetic routes of TCM-CP and TCM-CPS are illustrated in Scheme S1,† and the relative chemical structures were characterized using NMR spectroscopy and high-resolution mass spectrometry (ESI†).

Increasing hydrophilicity by forming a pyridinium salt

Photosensitizers with "off–on" fluorescence for image-guided PDT could realize high signal-to-noise ratio (S/N) imaging,
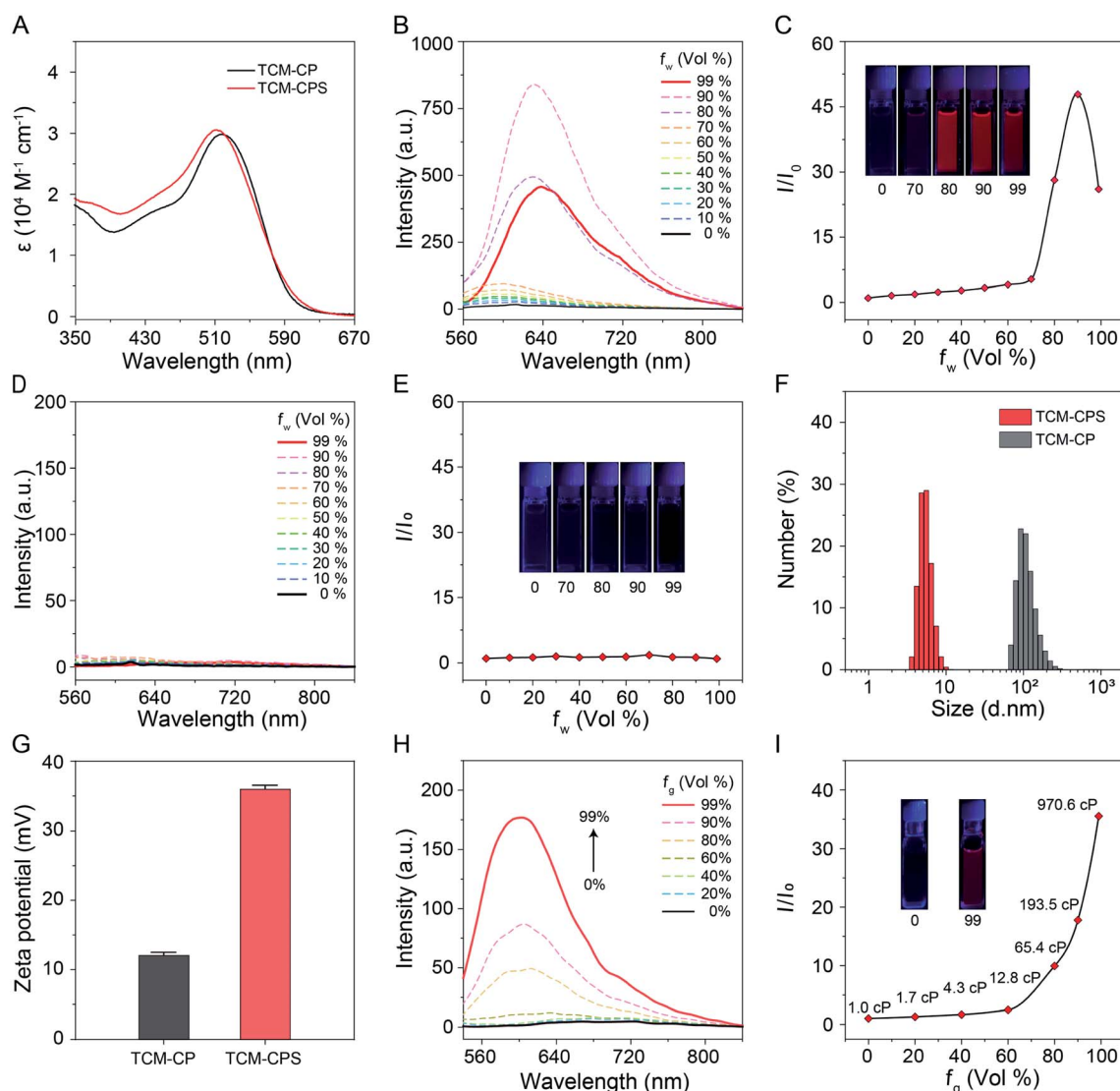

Fig. 2 AIE-active luminogens with enhanced solubility and stability in water when the pyridinium salt is formed. (A) Absorption spectra of TCM-CP and TCM-CPS in 99% water. (B) Fluorescence spectra and (C) I/I_0 plots of TCM-CP in THF–water mixtures with different water fractions. I_0 is the fluorescence intensity of the emission peak in THF, λ_{ex} = 520 nm. (D) Fluorescence spectra and (E) I/I_0 plots of TCM-CPS in THF–water mixtures with different water fractions. I_0 is the fluorescence intensity of the emission peak in THF, λ_{ex} = 520 nm. (F) Size distribution of TCM-CP and TCM-CPS in 99% water. (G) Comparison of zeta potentials in 99% water. (H) Fluorescence spectra and (I) I/I_0 plots of TCM-CPS in glycerol–water mixtures with different glycerol fractions. I_0 is the fluorescence intensity of the TCM-CPS emission peak in water, λ_{ex} = 520 nm. Concentrations of TCM-CP and TCM-CPS are 10 μM.

and long absorption and emission wavelengths for photosensitizers could improve the quality of imaging and therapy in deep tissue.[38–41] The photophysical properties of TCM-CP and TCM-CPS were examined using their absorption and emission spectra. The absorption peak of TCM-CP in 99% water was located at 518 nm, and the absorption peak of TCM-CPS (512 nm) was slightly blue-shifted compared to that of TCM-CP (Fig. 2A). Both compounds displayed very broad absorption, which is conducive to ROS generation under white light irradiation. Their AIE properties were then investigated in tetrahydrofuran (THF)–water mixtures. The fluorescence intensity of TCM-CP in THF was very weak (Fig. 2B) and increased gradually with increasing water fraction from 0 to 90% during the aggregation process. The emission peak of TCM-CP was redshifted with increasing water fraction, and was finally located at 638 nm in 99% water with 26.0 times the fluorescence intensity of that in THF (Fig. 2C), indicative of the typical AIE behavior of TCM-CP. Given that the introduction of the pyridinium salt increased the photosensitivity and dispersion in water, TCM-CPS showed little fluorescence in either THF or water under the same test conditions, which suggests low background fluorescence in bio-imaging (Fig. 2D and E). After increasing the slit width of the fluorescence spectrophotometer, TCM-CPS exhibited a low emission band at 678 nm with a large Stokes shift of 166 nm, and the emission peak of TCM-CPS was 40 nm longer than that of TCM-CP, which should favorably decrease the biological autofluorescence interference (Fig. S1†).

To explain the large difference between the fluorescence of TCM-CPS and TCM-CP in 99% water, their aggregation behaviors were investigated using dynamic light scattering (DLS) and transmission electron microscopy (TEM). As shown in Fig. 2F, the peak in the size distribution of TCM-CP occurred at 112.0 nm, while that of TCM-CPS was observed at 5.5 nm, illustrating the better dispersion of hydrophilic TCM-CPS. Also, according to the TEM images, their nanoparticles appeared to be spherical; the size of TCM-CPS was smaller than that of TCM-CP, and it showed more loose clusters in 99% water (Fig. S2†). Additionally, the zeta potential of TCM-CPS in water is 36.0 mV, which is larger than the zeta potential of 12.1 mV for TCM-CP (Fig. 2G and S3†), further illustrating the better colloidal stability of TCM-CPS in water. The DLS data, TEM images, and zeta potential results were consistent with their fluorescence intensity in water. After forming the pyridinium salt, the AIE-active luminogen TCM-CPS was obtained with enhanced hydrophilicity and colloidal stability in water, and exhibited lower fluorescence intensity in an aqueous system according to RIM.[42,43]

To further investigate the AIE property of TCM-CPS, the response of the fluorescence to viscosity was investigated in water–glycerin mixtures. The fluorescence intensity was obviously enhanced with increasing glycerin fraction due to the restricted motion of TCM-CPS resulting from the increase in the solution viscosity (Fig. 2H). The fluorescence intensity in 99% glycerol, with a viscosity of 970.6 cP, was 35.5 times higher than that in water, with a viscosity of 1.0 cP (Fig. 2I), indicating that TCM-CPS could sensitively respond to viscosity due to its AIE property.

Increasing photosensitivity and high free-radical ROS generation of TCM-CPS

The photosensitivity of TCM-CP and TCM-CPS were evaluated using commercially available photosensitizers as a positive control. The total ROS generation of the photosensitizers was detected using 2′,7′-dichlorodihydrofluorescein (DCFH) as an indicator. As shown in Fig. 3A and S4,† using commercially available Ce6 and RB as the photosensitizer, the fluorescence from the indicator at 525 nm increased 9.4 and 39.0 times upon light irradiation for 50 s, respectively. With TCM-CP as the photosensitizer, the fluorescence from the indicator increased 42.4 times, which was comparable to the increase for commercial RB and much higher than that for Ce6. In contrast, using TCM-CPS as the photosensitizer, the fluorescence from the indicator dramatically increased 96.5 times, and remained almost constant upon light irradiation for 50 s; this increase was much higher than those for TCM-CP, RB and Ce6, indicating that the highly efficient TCM-CPS had great potential to replace the commercial photosensitizers.

Time-dependent density functional theory (TD-DFT) calculations were then performed to explain why the total ROS generation was greatly increased upon forming pyridinium salt. As illustrated in Fig. 3B, the lowest unoccupied molecular orbital (LUMO) part of TCM-CPS was concentrated on the pyridinium salt group (acceptor), and the highest occupied molecular orbital (HOMO) part was concentrated on the carbazole groups (donor), indicating that pyridinium salt group mainly played the role of an "acceptor" in the D–π–A structure. The HOMO and LUMO distribution of TCM-CPS was greatly separated compared to the partial HOMO and LUMO distribution overlap of TCM-CP. The more separated HOMO–LUMO distribution led to smaller a ΔE_{ST} value, which could improve the triplet excited state yield, finally resulting in higher ROS generation.[44–46] Moreover, the singlet and triplet energy levels of both photosensitizers were further calculated and the energy gap between S_1 and T_1 ($\Delta E_{S1–T1}$) of TCM-CPS was 0.22 eV, which was much lower than that of TCM-CP (0.79 eV), facilitating the singlet–triplet ISC process (Fig. 3B and Table S1†). Above all, the separation of HOMO–LUMO to reduce $\Delta E_{S1–T1}$ can indeed facilitate the generation of ROS when the pyridinium salt is formed.

Type II photosensitizers undergo an energy-transfer mechanism to generate singlet oxygen ($^1O_2$), while type I photosensitizers undergo an electron-transfer mechanism to generate free-radical ROS in a less-oxygen-dependent manner.[47,48] In this work, multiple indicators were utilized to determine which type of ROS was produced by TCM-CPS. First, singlet oxygen sensor green (SOSG) was chosen to detect $^1O_2$. As shown in Fig. 3C and S5,† RB triggered high fluorescence of SOSG upon light irradiation for 4 min, while TCM-CPS triggered little fluorescence of SOSG with low $^1O_2$ production, suggesting poor $^1O_2$ generation by TCM-CPS. Thus, the efficient ROS generation of TCM-CPS was mainly attributed to the generation of free-radical ROS. Moreover, free-radical ROS generation was further verified by using the commercially available superoxide radical ($O_2^{-\bullet}$) fluorescent probe dihydrorhodamine 123 (DHR123) and the
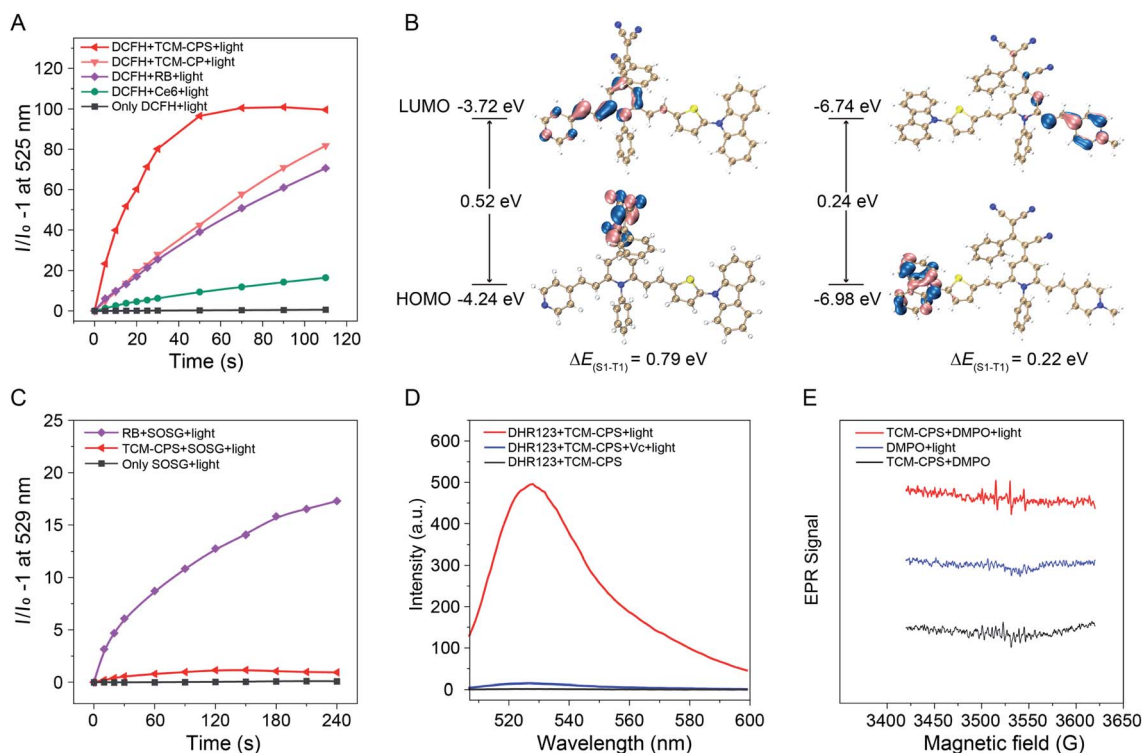
Fig. 3 TCM-CPS produces free radicals with high ROS generation. (A) Total ROS generation of TCM-CPS, TCM-CP, RB and Ce6 (10 μM) upon white light irradiation using DCFH (40 μM) as an indicator. I_0 is the fluorescence of the mixtures before light irradiation. $\lambda_{ex} = 488$ nm. (B) HOMO–LUMO distribution at S_1, energy gap between S_1 and T_1 for TCM-CP and TCM-CPS from TD-DFT (Gaussian/B3LYP/6-311G(d)). (C) Singlet oxygen generation of RB and TCM-CPS (10 μM) upon light irradiation using SOSG (10 μM) as an indicator. $\lambda_{ex} = 500$ nm. (D) Fluorescence spectra of the probe DHR123 (10 μM) for detecting free-radical ROS produced by TCM-CPS in the presence of vitamin C (100 μM) under light irradiation for 10 min. $\lambda_{ex} = 495$ nm. (E) ERP signals of DMPO after 3 min light irradiation for free-radical ROS characterization. Concentration: 1 mM for TCM-CPS and 200 mM for DMPO. Light (80 mW cm^{-2}, 400–650 nm); concentration of photosensitizers is 10 μM unless otherwise noted.

radical scavenger vitamin C (Vc).[49] As shown in Fig. 3D, RB triggers lower fluorescence intensity of DHR123 compared to TCM-CPS (Fig. S6 and S7†), and the addition of vitamin C only inhibits the fluorescence to 79.8%, confirming that RB is a type II photosensitizer. In contrast, TCM-CPS triggered high fluorescence of DHR123, and the fluorescence was seriously inhibited to 2.9% upon the addition of vitamin C, illustrating that the AIEgen-based TCM-CPS was a type I photosensitizer, that is, mainly producing free-radical ROS (Fig. 3D). Superoxide radicals can be converted to the highly cytotoxic hydroxyl radical ('OH);[24] these hydroxyl radicals were detected using hydroxyphenyl fluorescein (HPF) as an indicator. After irradiation, obvious fluorescence enhancement was observed in the mixture containing TCM-CPS and HPF, while the fluorescence of the mixtures without TCM-CPS remained almost unchanged after irradiation (Fig. S8†), further illustrating that TCM-CPS could efficiently produce free-radical ROS.

In addition, electron paramagnetic resonance (EPR) spectroscopy was used to detect free-radical ROS by using 5,5-dimethyl-1-pyrroline N-oxide (DMPO) as a spin trap. Upon light irradiation, the TCM-CPS solution with DMPO exhibited an obvious and characteristic EPR signal (Fig. 3E) suggestive of the generation of free-radical ROS. In contrast, no obvious EPR signal was observed under light irradiation alone or for TCM-CPS alone, which not only eliminated the possibility of background signal

from DMPO but also further confirmed that the generation of free-radical ROS required light irradiation. Compared to other reported type I photosensitizers,[50,51] TCM-CPS possesses two significant advantages, i.e., a very low initial fluorescence background and high ROS generation in water, which are critical for precise bio-imaging and efficient PDT. Above all, the total ROS production was greatly improved by separating the HOMO–LUMO to decrease ΔE_{S1-T1} and TCM-CPS could efficiently produce free-radical ROS upon light irradiation, indicating its promising application in hypoxic microenvironments.

Image-guided PDT of cancer cells with type I photosensitizer TCM-CPS

Considering large its Stokes shift, fluorescence activation in a motion-restricted microenvironment and highly efficient ROS production, TCM-CPS was expected to be able to realize image-guided PDT. As shown in Fig. 4A and S9,† strong red fluorescence was observed in the cells as clear dots upon incubation for 6 h, indicating that large amounts of TCM-CPS entered cells, and that the fluorescence was turned on in a motion-restricted microenvironment to image HeLa cells. Then, the intracellular ROS level was detected using 2′,7′-dichlorodihydrofluorescein diacetate (DCFH-DA) as a ROS indicator. Little green fluorescence from the indicator was observed in the HeLa cells
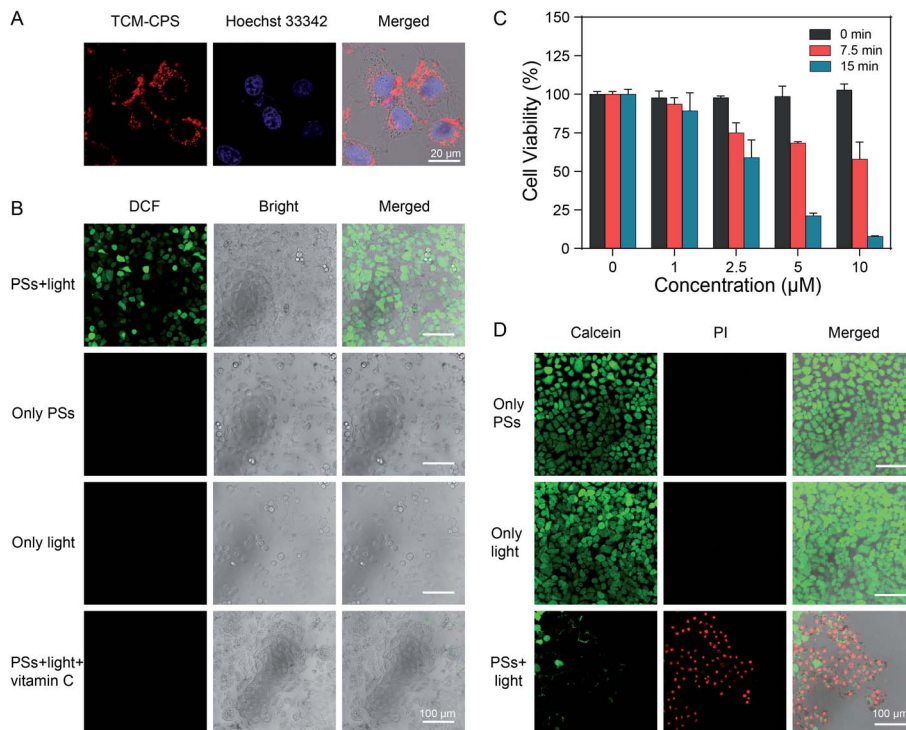
Fig. 4 TCM-CPS could efficiently kill HeLa cells through increasing the intracellular ROS level. (A) Confocal images of HeLa cells incubated with 10 μM TCM-CPS for 6 h, followed by incubation with 5 μg mL^{-1} Hoechst 33342 for 15 min. Red channel from TCM-CPS: $\lambda_{ex} = 514$ nm, $\lambda_{em} = 630$–750 nm, blue channel from Hoechst 33342: $\lambda_{ex} = 405$ nm, $\lambda_{em} = 415$–460 nm. Scale bar: 20 μm. (B) Intracellular ROS level in HeLa cells subjected to the various treatments as detected *via* the reaction between DCFH and ROS. Green channel from DCF: $\lambda_{ex} = 488$ nm, $\lambda_{em} = 505$–560 nm. Scale bar: 100 μm. (C) *In vitro* cytotoxicity of TCM-CPS in the dark and after 7.5 min and 15 min of white light irradiation. (D) Live–dead staining of HeLa cells subjected to the various treatments. The live cells were stained with 2 μM calcein-AM for 20 min, while the dead cells were stained with 4.5 μM propidium iodide (PI) for 20 min. Green channel from calcein: $\lambda_{ex} = 488$ nm, $\lambda_{em} = 495$–540 nm, red channel from PI: $\lambda_{ex} = 561$ nm, $\lambda_{em} = 590$–650 nm. Scale bar: 100 μm. Light: 40 mW cm^{-2}, 400–650 nm, PSs: photosensitizers.

incubated with photosensitizers alone (without light) or under light irradiation alone (without photosensitizers). On the contrary, HeLa cells incubated sequentially with TCM-CPS (10 μM) for 6 h, DCFH-DA (20 μM) for 20 min, and light irradiation for 5 min exhibited bright green fluorescence (Fig. 4B), which was indicative of an increase in the intracellular ROS level. The green fluorescence was dramatically decreased when the cells were pretreated with the free radical scavenger vitamin C, further illustrating that TCM-CPS is a type I photosensitizer and mainly produces free-radical ROS in cells.

MTT assay was carried out to evaluate the cell viability in the dark and under light irradiation. As shown in Fig. 4C, after incubation with 10 μM TCM-CPS, about 100% cell viability was observed without irradiation, which was indicative of good biocompatibility. The cell viability decreased to 58.0% upon irradiation for 7.5 min, and to 7.9% upon irradiation for 15 min, illustrating the effective cell lethality of TCM-CPS. The cell viability exhibited concentration- and light irradiation time-dependence. To further intuitively visualize the PDT efficiency of TCM-CPS, calcein-AM and propidium iodide (PI) were used to distinguish live (green) and dead (red) cells. After pre-treatment with TCM-CPS and irradiation with light, strong red fluorescence and a little green fluorescence were observed in the cells, indicating that TCM-CPS could effectively kill cells in

combination with light irradiation. On the contrary, strong green fluorescence and almost no red fluorescence in the cells was observed in the TCM-CPS incubation alone and light irradiation alone groups, which was indicative of the good biocompatibility of TCM-CPS (Fig. 4D). The *in vitro* cytotoxicity of TCM-CPS under hypoxic conditions was further evaluated. In an extremely hypoxic environment, the cell viability decreased to 50.7% upon irradiation for 15 min with TCM-CPS (15 μM), illustrating that TCM-CPS could produce obvious cell toxicity in an extremely hypoxic environment (Fig. S10†). Above all, TCM-CPS could enter and image cancer cells, and increase the intracellular ROS level under light irradiation, thus efficiently killing HeLa cells at a low concentration.

Quick binding to and efficient killing of G− and G+ bacteria with TCM-CPS

The abuse of antibiotics can induce many drug-resistant bacteria, which seriously harms human health. As a new broad-spectrum therapy, PDT has the advantages of controllable treatment area and no drug resistance in killing bacteria. Herein, *Escherichia coli* (*E. coli*) and *Staphylococcus aureus* (*S. aureus*) were chosen as representative Gram-negative (G−) and Gram-positive (G+) bacteria to verify the treatment effect of TCM-CPS. First, its imaging capability was investigated by

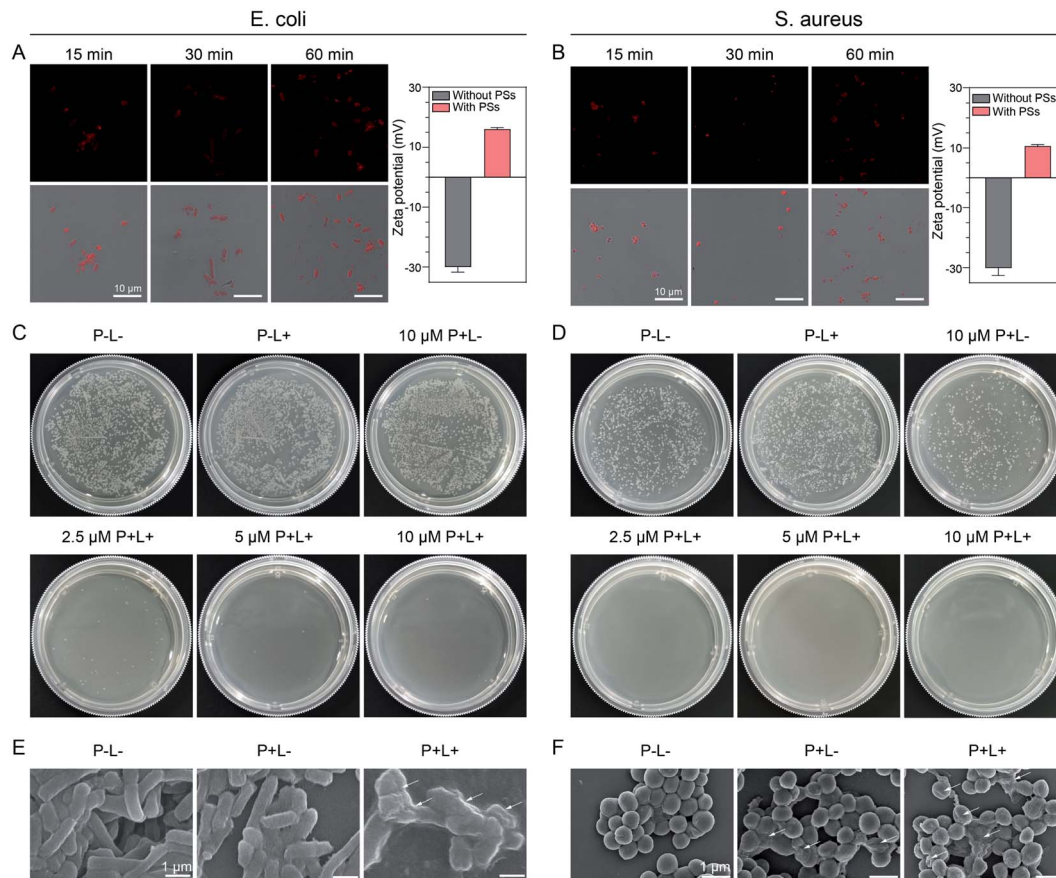**Fig. 5** TCM-CPS quickly binds to the surface of bacteria through electrostatic interaction and efficiently kills both G− and G+ bacteria at a low concentration. (A) Confocal images of *E. coli* and (B) *S. aureus* with different TCM-CPS (10 μM) incubation times. λ_{ex} = 514 nm, λ_{em} = 650–750 nm. Scale bar: 10 μm. (A right) Zeta potential of *E. coli* and (B right) *S. aureus* with or without incubation with TCM-CPS (10 μM) in water. (C) Plate photographs of *E. coli* and (D) *S. aureus* colonies. The bacteria were incubated with different concentrations of TCM-CPS for 30 min, and then irradiated with light for 15 min or kept in the dark. The bacteria solution was coated on an LB agar plate, and the plates were then photographed after another 12 h of incubation. P+: with photosensitizer, L+: irradiation with light, P−: without photosensitizer, L−: without light. (E) SEM images of *E. coli* and (F) *S. aureus* subjected to the different treatments. The concentration of TCM-CPS is 10 μM, and the irradiation time is 15 min. Scale bar: 1 μm. Light: 40 mW cm^{-2}, 400–650 nm.

incubating the bacteria with 10 μM TCM-CPS for 15 min. As shown in Fig. 5A, bright fluorescence with hollow rod-like shapes appeared for the *E. coli*, and bright fluorescence with round shapes appeared for *S. aureus* (Fig. 5B), indicating that TCM-CPS could quickly bind to both *E. coli* and *S. aureus*, thus realizing fluorescence imaging. Then, the electrostatic interaction between the bacteria and TCM-CPS was proved using a zeta potential test. Specifically, the zeta potential was −30.0 mV for *E. coli*, and 36.0 mV for TCM-CPS. After incubation with TCM-CPS, the zeta potential of *E. coli* increased to +16.1 mV (Fig. 5A), and that of *S. aureus* increased from −30.1 to +10.6 mV (Fig. 5B). Thus, the AIEgen-based TCM-CPS could bind to bacteria quickly through electrostatic interaction and realize rapid fluorescence imaging of the bacteria.

Rapid binding to the bacteria and high ROS generation made the killing of bacteria with TCM-CPS possible. We conducted a sterilization experiment by incubating the bacteria with different concentrations of TCM-CPS for 30 min, exposing them to white light irradiation for 15 min, and culturing them for another 12 h at 37 °C, followed by imaging and colony counting.

As indicated in Fig. 5C, the number of *E. coli* bacterial colonies dramatically decreased after incubation with the TCM-CPS in a concentration-dependent manner, in contrast with the large quantities of colonies in the negative control group (P−L−, no TCM-CPS in the dark) and P−L+ group (no TCM-CPS with light irradiation). In particular, very few colonies of *E. coli* were found at a 2.5 μM photosensitizer concentration with irradiation, indicating that TCM-CPS at a low concentration was effective enough to kill the *E. coli*. In addition, the 10 μM TCM-CPS group had similar colony numbers to the negative control group, illustrating that TCM-CPS did not affect the *E. coli* activity without light irradiation. A similar phenomenon was observed for *S. aureus*, with the number of bacterial colonies decreasing upon incubation with TCM-CPS in a concentration-dependent manner (Fig. 5D). The toxicity of TCM-CPS to *S. aureus* was stronger than that to *E. coli*. The difference was that some *S. aureus* could be killed by TCM-CPS without irradiation because the outer membrane of *S. aureus* provided less protection than that of *E. coli*.[52] Above all, TCM-CPS could kill both *E. coli* and *S. aureus* efficiently at a low concentration under light irradiation.

The morphological changes in the bacteria with and without light irradiation were observed through scanning electron microscopy (SEM). As shown in Fig. 5E, the *E. coli* in the P−L− group showed a smooth and plump rod shape, and the morphology of *E. coli* in the P+L− group (10 μM TCM-CPS) was almost the same as that in the P−L− group, indicating that the 10 μM TCM-CPS shows little toxicity toward *E. coli* in the dark. Upon incubation with 10 μM TCM-CPS followed with 15 min of light irradiation, the morphology of *E. coli* became sunken and rough, indicating that the ROS produced by TCM-CPS could severely damage the *E. coli*. Similarly, the *S. aureus* in the P−L− group showed a plump spherical shape. After incubation with TCM-CPS followed by a period of darkness, some of the *S. aureus* became sunken, indicating that TCM-CPS showed a little toxicity in the dark. Upon incubation with TCM-CPS followed by light irradiation, the morphology of many *S. aureus* became sunken and even collapsed, indicating that TCM-CPS could efficiently damage *S. aureus* under light irradiation (Fig. 5F). Thus, TCM-CPS can kill both G− and G+ bacteria at a low concentration.

Accelerated wound healing process with decreased infection in mice

Based on the excellent bacteria killing efficiency of TCM-CPS, its use in the PDT treatment modality for bacteria-infected wounds was further investigated. A skin biopsy punch was used to create wounds on the backs of mice, and 20 μL *E. coli* (10^8 CFU mL^{-1}) was used to infect the wounds for 2 h. In the PDT group, the wounds were dripped with 30 μL TCM-CPS (20 μM in PBS, one incubation period of 15 min) twice, followed by white light irradiation for 15 min. In the PBS group, the wounds were only dripped with 30 μL PBS twice. Photos of the wounds were taken at day 0, 2, 4, 7, 9, and 11 (Fig. 6A and B), and the change in their relative size was recorded (Fig. 6C). In the PBS group, obvious symptoms of infection were observed around the wounds in two mice (white squares in Fig. 6A), while there were no obvious symptoms of infection around the wounds in the PDT group, indicating that PDT therapy greatly decreased wound infection. As shown in Fig. 6C, the relative size of the wounds on day 2 was about 60% in the PBS group, while it was about 32% in the PDT group, and the relative size of wounds in the PDT group was always smaller than that in the PBS group after treatment, indicating that the healing of the wounds in the PDT group was faster than that in the PBS group.

To verify that the bacteria were efficiently killed though PDT therapy, the mice were sacrificed at day 4, and the wound tissue was homogenized with PBS. After dilution, the solution was coated on a Luria–Bertani (LB) agar plate. As shown in Fig. 6D, the colony number in the wound tissue significantly decreased
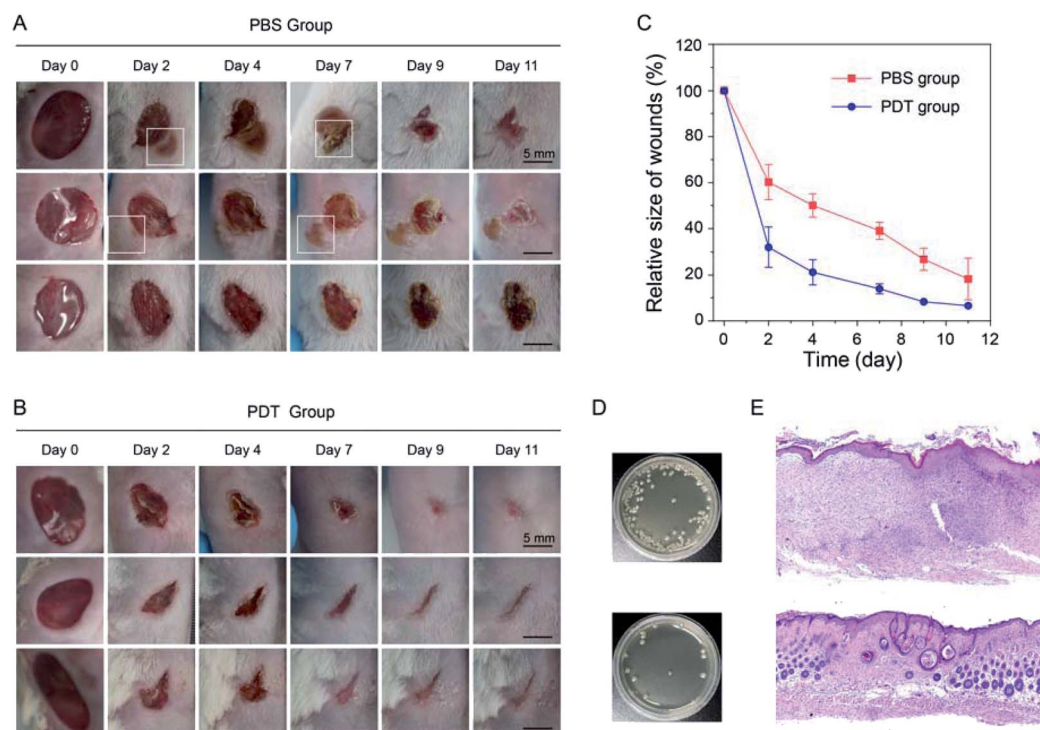

Fig. 6 TCM-CPS could accelerate the wound healing process and decrease wound infection in mice *via* PDT. (A) The wound was infected with 20 μL *E. coli* (10^8 CFU mL^{-1}) for 2 h and then treated with PBS. (B) After infection, the wound was treated with 30 μL TCM-CPS (20 μM in PBS, one incubation period of 15 min) twice, followed by white light irradiation (40 mW cm^{-2}, 400−650 nm) for 15 min. Photos of the wound were taken at day 0, 2, 4, 7, 9, and 11, and all photos in the PBS and PDT groups share the same scale bar of 5 mm. (C) The scar area *versus* time, setting the wound area at day 0 as 100%; data are shown as mean ± s.d. with $N = 3$. (D) The wound tissue from the PBS or PDT group was sampled on day 4 and then homogenized with PBS. The diluted supernatant liquid of the tissue homogenate was coated on an LB agar plate (top: PBS group; bottom: PDT group). (E) H&E staining of wound tissue sampled at day 11 (top: PBS group; bottom: PDT group); the magnification is 50 times.

after PDT therapy, which was consistent with the obvious decrease in bacterial infection after PDT therapy. To compare the wound healing between the PBS group and PDT group in depth, the mice were sacrificed at day 11, and the hematoxylin and eosin (H&E) staining of the wound tissue was performed (Fig. 6E). Large skin wound healing areas, epidermal hyperplasia with hyperkeratosis, intradermal interstitial edema, and granulation tissue hyperplasia were observed in the PBS treatment group, along with a large number of infiltrating lymphocytes, plasma cells and neutrophils. However, in the PDT treatment group, the skin wound was healed with a smaller scar area, the epidermis was mildly proliferated with keratinous sac formation, and the fibrous tissue in the dermis was proliferated, along with the infiltration of a small number of lymphocytes and plasma cells. H&E staining further proved the healing effect of PDT group. Thus, TCM-CPS could accelerate the wound healing process and decrease the bacterial infection of the wounds though PDT therapy.

Conclusions

We reported an AIEgen TCM-based type I photosensitizer with NIR emission and "off–on" fluorescence via rational molecular design, which was expected to achieve precise imaging and low oxygen dependence in the image-guided PDT modality. The strongly electron-donating carbazole unit and π-bridged thiophene were introduced to extend the wavelength, and the hydrophilic pyridinium salt unit was introduced to maintain the fluorescence-off state in an aqueous system. The strong D–π–A structure in TCM-CPS can not only ensure strong ICT for NIR emission but also greatly separate the HOMO–LUMO distribution for high ROS production. As demonstrated via fluorescence and EPR methods, TCM-CPS showed much higher ROS generation than the commercially available photosensitizers Ce6 and RB under white light irradiation, indicating that it was a highly efficient free-radical ROS photogenerator with highly desirable applications in hypoxic environments. Due to its high hydrophilicity and photosensitivity, TCM-CPS could enter cells and increase the intracellular ROS level upon light irradiation, thus efficiently killing cancer cells. Positively charged TCM-CPS could bind to negatively charged bacteria quickly via electrostatic interactions and kill both Gram-negative and Gram-positive bacteria at a low concentration. Bacteria-infected wounds in mice showed an accelerated wound healing process and decreased wound infection after PDT treatment. The type I photosensitizer TCM-CPS with NIR emission and "off–on" fluorescence has great potential in image-guided PDT for the treatment of cancer and bacterial infection.

Data availability

All relevant data is presented in the paper and ESI.†

Author contributions

Z. Liu, Q. Wang, and W. H. Zhu conceived the study, designed the experimental work, analysed the results and revised the manuscript. Z. Liu performed experimental work and wrote the manuscript. W. Qiu, Y. Lyu, Z. Zhu and X. Zhao designed the bio-experiment and analysed the bio-experiment results.

Conflicts of interest

There are no conflicts to declare.

Acknowledgements

Notes and references

1 D. Dolmans, D. Fukumura and R. K. Jain, Nat. Rev. Cancer, 2003, 3, 380–387.

2 A. P. Castano, P. Mroz and M. R. Hamblin, Nat. Rev. Cancer, 2006, 6, 535–545.

3 B. Wang, M. Wang, A. Mikhailovsky, S. Wang and G. C. Bazan, Angew. Chem., Int. Ed., 2017, 56, 5031–5034.

4 F. Xu, H. Ge, N. Xu, C. Yang, Q. Yao, S. Long, W. Sun, J. Fan, X. Xu and X. Peng, Sci. China: Chem., 2021, 64, 488–498.

5 S. Guo, M. Han, R. Chen, Y. Zhuang, L. Zou, S. Liu, W. Huang and Q. Zhao, Sci. China: Chem., 2019, 62, 1639–1648.

6 W. Zhai, Y. Zhang, M. Liu, H. Zhang, J. Zhang and C. Li, Angew. Chem., Int. Ed., 2019, 58, 16601–16609.

7 H. Chen, S. Li, M. Wu, Kenry, Z. Huang, C.-S. Lee and B. Liu, Angew. Chem., Int. Ed., 2020, 59, 632–636.

8 H. Wu, F. Zeng, H. Zhang, J. Xu, J. Qiu and S. Wu, Adv. Sci., 2016, 3, 1500254.

9 W. Wu, D. Mao, S. Xu, M. Panahandeh-Fard, Y. Duan, F. Hu, D. Kong and B. Liu, Adv. Funct. Mater., 2019, 29, 1901791.

10 J. Ge, M. Lan, B. Zhou, W. Liu, L. Guo, H. Wang, Q. Jia, G. Niu, X. Huang, H. Zhou, X. Meng, P. Wang, C.-S. Lee, W. Zhang and X. Han, Nat. Commun., 2014, 5, 4596.

11 G. Feng and B. Liu, Acc. Chem. Res., 2018, 51, 1404–1414.

12 J. F. Lovell, C. S. Jin, E. Huynh, H. Jin, C. Kim, J. L. Rubinstein, W. C. W. Chan, W. Cao, L. V. Wang and G. Zheng, Nat. Mater., 2011, 10, 324–332.

13 B. Li, J. Li, Y. Fu and Z. Bo, J. Am. Chem. Soc., 2004, 126, 3430–3431.

14 J. F. Lovell, T. W. B. Liu, J. Chen and G. Zheng, Chem. Rev., 2010, 110, 2839–2857.

15 X. Li, N. Kwon, T. Guo, Z. Liu and J. Yoon, Angew. Chem., Int. Ed., 2018, 57, 11522–11531.

16 J. M. Brown and W. R. Wilson, Nat. Rev. Cancer, 2004, 4, 437–447.

17 F. Hu, S. Xu and B. Liu, Adv. Mater., 2018, 30, 1801350.

18 Z. Liu, H. Zou, Z. Zhao, P. Zhang, G.-G. Shan, R. T. K. Kwok, J. W. Y. Lam, L. Zheng and B. Z. Tang, ACS Nano, 2019, 13, 11283–11293.

19 Q. Li, Y. Li, T. Min, J. Gong, L. Du, D. L. Phillips, J. Liu, J. W. Y. Lam, H. H. Y. Sung, I. D. Williams, R. T. K. Kwok, C. L. Ho, K. Li, J. Wang and B. Z. Tang, *Angew. Chem., Int. Ed.*, 2020, **59**, 9470–9477.

20 Z. Zhang, W. Xu, M. Kang, H. Wen, H. Guo, P. Zhang, L. Xi, K. Li, L. Wang, D. Wang and B. Z. Tang, *Adv. Mater.*, 2020, **32**, 2003210.

21 X. Zhang, Y. Chen, C. Li, Z. Xue, H. Wu, J. Li, H. Ou, J. Shen and D. Ding, *ACS Appl. Bio Mater.*, 2021, **4**, 3796–3804.

22 J. Mei, N. L. C. Leung, R. T. K. Kwok, J. W. Y. Lam and B. Z. Tang, *Chem. Rev.*, 2015, **115**, 11718–11940.

23 Y. Xie and Z. Li, *Natl. Sci. Rev.*, 2020, **8**, nwaa199.

24 Q. Wan, R. Zhang, Z. Zhuang, Y. Li, Y. Huang, Z. Wang, W. Zhang, J. Hou and B. Z. Tang, *Adv. Funct. Mater.*, 2020, **30**, 2002057.

25 W. Fu, C. Yan, Z. Guo, J. Zhang, H. Zhang, H. Tian and W.-H. Zhu, *J. Am. Chem. Soc.*, 2019, **141**, 3171–3177.

26 Z. Zhu, Q. Wang, H. Liao, M. Liu, Z. Liu, Y. Zhang and W.-H. Zhu, *Natl. Sci. Rev.*, 2020, **8**, nwaa198.

27 J. Zhang, Q. Wang, Z. Guo, S. Zhang, C. Yan, H. Tian and W.-H. Zhu, *Adv. Funct. Mater.*, 2019, **29**, 1808153.

28 T. Zhou, Q. Wang, M. Liu, Z. Liu, Z. Zhu, X. Zhao and W.-H. Zhu, *Aggregate*, 2021, **2**, e22.

29 Z. Liu, Q. Wang, Z. Zhu, M. Liu, X. Zhao and W.-H. Zhu, *Chem. Sci.*, 2020, **11**, 12755–12763.

30 J. Zhang, Q. Wang, J. Liu, Z. Guo, J. Yang, Q. Li, S. Zhang, C. Yan and W.-H. Zhu, *ACS Appl. Bio Mater.*, 2019, **2**, 943–951.

31 M. Gao, F. Yu, C. Lv, J. Choo and L. Chen, *Chem. Soc. Rev.*, 2017, **46**, 2237–2271.

32 J. Huang, C. Xie, X. Zhang, Y. Jiang, J. Li, Q. Fan and K. Pu, *Angew. Chem., Int. Ed.*, 2019, **58**, 15120–15127.

33 Kenry, Y. Duan and B. Liu, *Adv. Mater.*, 2018, **30**, 1802394.

34 J. Chen, L. Chen, Y. Wu, Y. Fang, F. Zeng, S. Wu and Y. Zhao, *Nat. Commun.*, 2021, **12**, 6870.

35 X. Gu, R. T. K. Kwok, J. W. Y. Lam and B. Z. Tang, *Biomaterials*, 2017, **146**, 115–135.

36 H. Ou, S. Dai, R. Liu and D. Ding, *Sci. China: Chem.*, 2019, **62**, 929–932.

37 M. Kang, Z. Zhang, N. Song, M. Li, P. Sun, X. Chen, D. Wang and B. Z. Tang, *Aggregate*, 2020, **1**, 80–106.

38 H. Lin, Z. Lin, K. Zheng, C. Wang, L. Lin, J. Chen and J. Song, *Adv. Opt. Mater.*, 2021, **9**, 2002177.

39 G. Hong, A. L. Antaris and H. Dai, *Nat. Biomed. Eng.*, 2017, **1**, 0010.

40 Q. Chen, J. Chen, Z. Yang, L. Zhang, Z. Dong and Z. Liu, *Nano Res.*, 2018, **11**, 5657–5669.

41 H. Bian, D. Ma, X. Zhang, K. Xin, Y. Yang, X. Peng and Y. Xiao, *Small*, 2021, **17**, 2100398.

42 Y. Zhang, Q. Wang, Z. Zhu, W. Zhao, C. Yan, Z. Liu, M. Liu, X. Zhao, H. Tian and W.-H. Zhu, *CCS Chem.*, 2021, **3**, 1800–1813.

43 Z. Guo, C. Yan and W.-H. Zhu, *Angew. Chem., Int. Ed.*, 2020, **59**, 9812–9825.

44 C. Chen, X. Ni, S. Jia, Y. Liang, X. Wu, D. Kong and D. Ding, *Adv. Mater.*, 2019, **31**, 1904914.

45 S. Xu, Y. Yuan, X. Cai, C.-J. Zhang, F. Hu, J. Liang, G. Zhang, D. Zhang and B. Liu, *Chem. Sci.*, 2015, **6**, 5824–5830.

46 J. Li, H. Gao, R. Liu, C. Chen, S. Zeng, Q. Liu and D. Ding, *Sci. China: Chem.*, 2020, **63**, 1428–1434.

47 P. R. Ogilby, *Chem. Soc. Rev.*, 2010, **39**, 3181–3209.

48 M. S. Baptista, J. Cadet, P. Di Mascio, A. A. Ghogare, A. Greer, M. R. Hamblin, C. Lorente, S. C. Nunez, M. S. Ribeiro, A. H. Thomas, M. Vignoni and T. M. Yoshimura, *Photochem. Photobiol.*, 2017, **93**, 912–919.

49 M. Li, T. Xiong, J. Du, R. Tian, M. Xiao, L. Guo, S. Long, J. Fan, W. Sun, K. Shao, X. Song, J. W. Foley and X. Peng, *J. Am. Chem. Soc.*, 2019, **141**, 2695–2702.

50 J. Tian, M. Teng, M. Song, Z. Li, X. Zhang and Y. Xu, *Dyes Pigm.*, 2021, **194**, 109651.

51 Y.-F. Xiao, W.-C. Chen, J.-X. Chen, G. Lu, S. Tian, X. Cui, Z. Zhang, H. Chen, Y. Wan, S. Li and C.-S. Lee, *ACS Appl. Mater. Interfaces*, 2022, **14**, 5112–5121.

52 Y. Huang, H. C. Pappas, L. Zhang, S. Wang, R. Cai, W. Tan, S. Wang, D. G. Whitten and K. S. Schanze, *Chem. Mater.*, 2017, **29**, 6389–6395.